catalysts

MDPI

Article

Photoactive Hybrid Film Photocatalyst of Polyethersulfone-ZnO for the Degradation of Methyl Orange Dye: Kinetic Study and Operational Parameters

Zul Adlan Mohd Hir [1,2], Abdul Halim Abdullah [1,2,*], Zulkarnain Zainal [2] and Hong Ngee Lim [2]

1 Materials Synthesis and Characterization Laboratory, Institute of Advanced Technology, Universiti Putra Malaysia, Serdang 43400 UPM, Selangor, Malaysia; zuladlan@gmail.com

2 Department of Chemistry, Faculty of Science, Universiti Putra Malaysia, Serdang 43400 UPM, Selangor, Malaysia; zulkar@upm.edu.my (Z.Z.); hongngee@upm.edu.my (H.N.L.)

* Correspondence: halim@upm.edu.my; Tel.: +60-12-270-3483

Received: 5 October 2017; Accepted: 23 October 2017; Published: 26 October 2017

Abstract: A facile and effective technique to immobilize photocatalyst nanoparticles by incorporating zinc oxide (ZnO) into polyethersulfone polymeric films by means of a phase inversion technique is reported. The degradation study of methyl orange (MO) dye was performed using a series of ZnO-embedded polymer hybrid systems. The photoactivity of the films increased in parallel with increased ZnO loading up to 17 wt%. The photodegradation process followed a pseudo first-order kinetics with an achievement of almost 100% MO removal in original conditions. The PZ-17 film demonstrated an excellent and comparable degradation performance up to five cycles, signifying the reliability of the film photocatalyst against ultraviolet irradiation and degradation.

Keywords: zinc oxide; polyethersulfone; phase inversion; film photocatalyst; methyl orange

1. Introduction

Wastewaters from industrial, commercial, and residential regions are responsible for the presence of a significant amount of organic contaminants in our water streams today [1,2]. Most of the artificial dyes commonly employed in the production of paper, plastics, leather, textiles, and cosmetic products today are toxic and non-biodegradable [3–5]. During the manufacturing process, some of the dyes are discharged as effluents, thus causing a severe threat to the environment. Due to their hazardous nature, the existence of these contaminants in our waters and surrounding ecosystem has increased public health issues [6]. Hence, the immediate challenge is to find effective methods for the treatment of the wastewaters.

The conventional approach to mitigate dyes from wastewater such as sedimentation, adsorption, filtration, and coagulation only transfers the dyes from one stage to another, hence generating secondary pollution [7,8]. Advanced approaches such as photocatalysis have been reported to degrade recalcitrant organic pollutants from wastewaters into harmless end products in the presence of ZnO and TiO_2 photocatalysts [9–12]. Nonetheless, this technique suffered from some technical aspects that impeded its industrial production, i.e., the ineffective utilization of ultraviolet or visible light due to agglomeration, reduced adsorption performance for hydrophobic pollutants, inhomogeneous dispersion in aqueous suspensions, and post-retrieval of the nanoparticles after the degradation process [13].

The separation of the photocatalysts from the substrate can be realized by means of membrane separation, immobilization on a polymer support or magnetic approach [13–16]. Earlier studies

demonstrated that the use of a polymer resin such as polyethersulfone (PES) as a support allowed more stability under ultraviolet exposure, where the resin was not simply degraded by hydroxyl radicals formed during the process and was marked as the right candidate for support materials in photocatalysis [17,18]. The incorporation of nanoparticles inside the PES matrix simultaneously improved its physicochemical properties such as surface hydrophilicity, as well as thermal and mechanical durability.

Recently, researchers successfully prepared PES/TiO_2 film photocatalysts that exhibited good photocatalytic performance in degrading methyl orange dye solution [19]. Several studies reported that ZnO exhibited better photocatalytic activity than TiO_2 in the degradation of some organic compounds. The biggest advantage of using ZnO is that it absorbs over a larger fraction of the solar/UV spectrum than TiO_2. Theoretically, the large band gap of ZnO of 3.37 eV has a high exciton binding energy of 60 meV at room temperature, which can exhibit semiconducting and piezoelectric dual properties. When ZnO is illuminated with UV radiation, electron–hole pairs are simultaneously generated within the metal oxide semiconductor. The valence band hole has an intensive reduction potential and it leads to the generation of more •OH radicals (as compared to TiO_2) that are known to be powerful and non-selective oxidizing agents, responsible for superior photocatalytic degradation activity [2,20,21]. Therefore it was hypothesized that the incorporation of the appropriate amount of ZnO into PES could yield a better performance than PES/TiO_2 film photocatalyst. However, a detailed study exploring the preparation of hybrid film photocatalyst incorporating high ZnO nanoparticles into PES has not been studied to the best of our knowledge, especially in the field of the photocatalysis process. Therefore, the purpose of the current work was to develop PES/ZnO hybrid film photocatalysts and to examine the effect of formulation on the physicochemical properties of the ZnO blended PES. Emphasis was placed on the photoactivity of PES/ZnO film photocatalysts in degrading methyl orange dyes in various operational parameters which include initial pH, initial concentration, and quantity of film. Moreover, the recyclibility study was also systematically elucidated by using the best PES/ZnO film photocatalyst in the photocatalytic degradation process.

2. Results and Discussion

2.1. X-ray Diffraction Analysis

The crystallinity and phase formation of pristine PES and certain PES/ZnO film photocatalysts are shown in Figure 1. The samples were labelled as per Table 5 in Section 3.2 below. No peaks were identified in the X-ray diffraction (XRD) spectrums for pristine PES indicating the amorphous nature of the film (Figure 1a). For the PES/ZnO films, several peaks characteristic of the ZnO hexagonal structure according to the Joint Committee on Powder Diffraction Standard (JCPDS) card no. 36-1451 were observed (Figure 1b–d), indicating the successful immobilization of ZnO into the PES matrix. The crystallinity of the ZnO peaks on diffraction plane (100, 002, and 101) increased in parallel with the increase in the amount of ZnO deposited into PES. Furthermore, there were no substantial changes of the peaks' intensities signifying that the PES had not experienced modifications in term of the crystallographic structure of ZnO nanoparticles after their incorporation into the PES matrix. Particularly, the diffracted peak at (101) is more intense than the peak at (002) and (101) orientation. This specifies that the nanocrystals formation has a preferred crystallographic at (101) orientation [22]. Thus, the crystallite size was estimated from the average peak width of (101) using the Scherrer equation and was equal to 55 nm for all prepared samples.

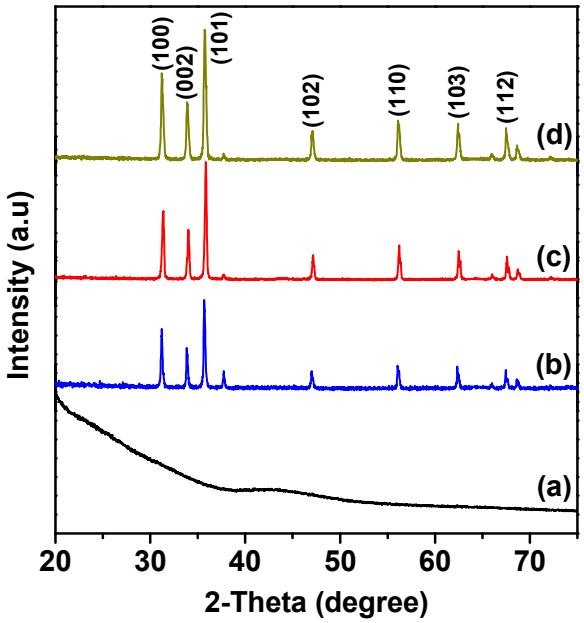

Figure 1. X-ray diffraction patterns of (**a**) PZ-0, (**b**) PZ-9, (**c**) PZ-17, and (**d**) PZ-19.

2.2. Surface Morphological and Structural Analysis

The scanning electron microscopy (SEM) technique, fitted with an energy dispersive X-ray (EDX) analyzer was employed to evaluate the surface morphological and cross-section of the resultant hybrid film photocatalysts and their elemental compositions, respectively. Figure 2 shows the surface morphology of the pristine PES (Figure 2a) and PES-ZnO films (Figure 2c,e,g). It was noticeable that upon the addition of the ZnO nanoparticles into the PES, there was a good distribution of ZnO nanoparticles inside the PES matrix but agglomeration occurred when the ZnO loading was increased above 17 wt%. This could be attributed to the viscosity of the polymer solution that intensified with an increase in ZnO loading, thus causing a reduction in the dispersion of the ZnO nanoparticles which in turn led to the development of large, aggregated ZnO particles inside the polymer matrix [23,24]. The EDX spectrums of the PES/ZnO film photocatalysts (Figure 2b,d,f,h), revealed the presence of immobilized ZnO with increased ZnO loading in the films.

The cross-sectional SEM micrographs (Figure 3) depicted a porous structure of the films that consisted of finger-like and tear-like microvoids on the pristine PES and the films with a higher loading of ZnO nanoparticles, respectively. The generation of a porous substructure with finger-like microvoids could be attributed to the instantaneous phase inversion that took place during the preparation of the films [25,26]. The porosity of the films also increased with increased ZnO loading from 0.04% (pristine PES) to 0.23% (PZ-17). However, a slight decrease in porosity to 0.20% was observed in the film with a higher ZnO loading (PZ-19). This could be due to the occurrence of agglomerated and bulky ZnO particles that might have damaged the polymer network structure and by limiting its movements, thus initiating the formation of a film with least porosity. The existence of excess ZnO particles in the matrix could also lead to a decrease in the porosity of the film [24,27]. Figure 4 displays the three dimensional atomic force microscopy (AFM) photographs of the pristine PES and PZ-17 films based on a sample size area of 2 μm × 2 μm. The surface roughness of PZ-17, as determined by AFM analysis software, was higher than that of pristine PES with mean surface roughness values of 13.80 nm and 2.19 nm, respectively. This phenomenon is due to the cluster's size formation on the surface of the film as a consequence of agglomeration of the nanoparticles [28].

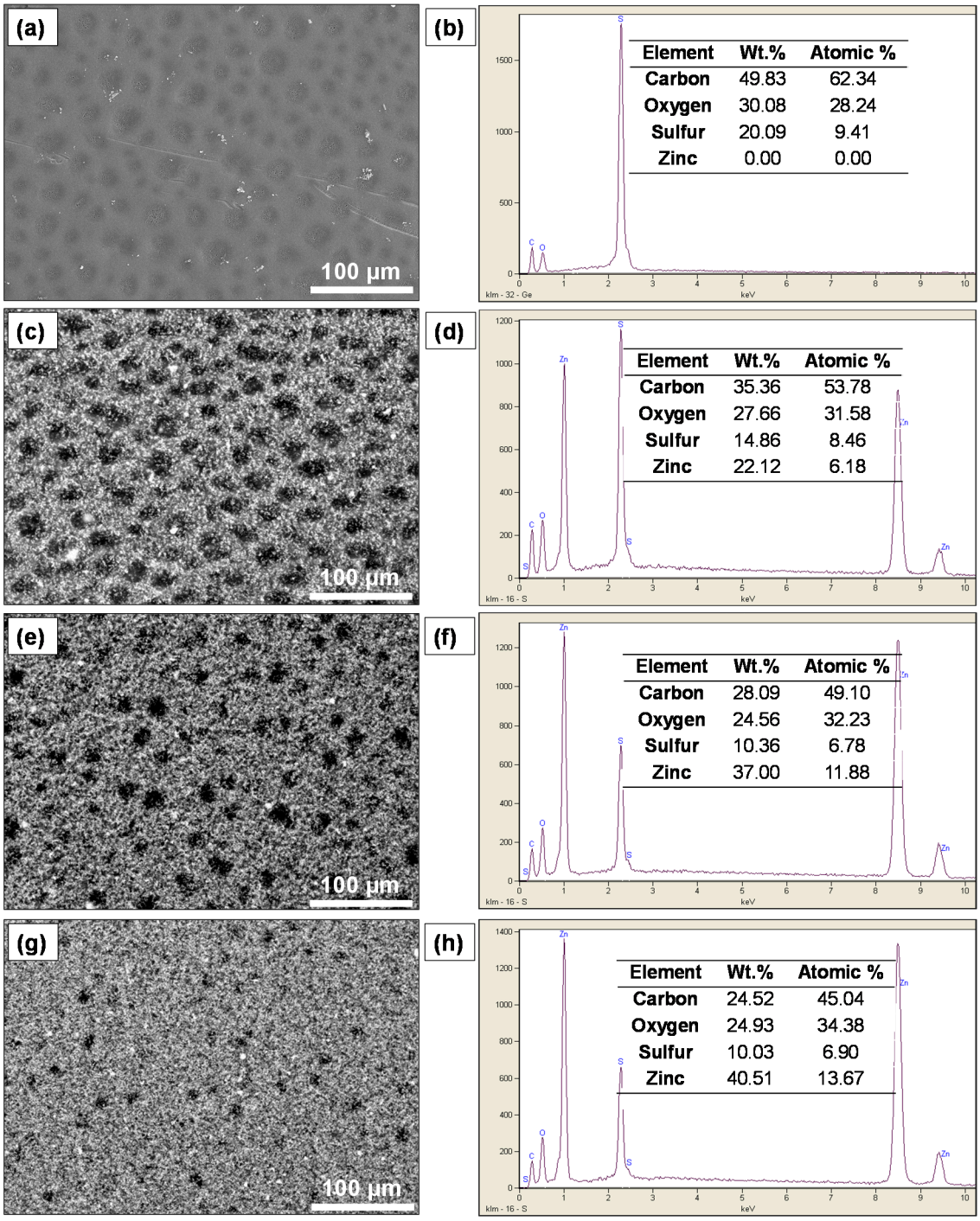

Figure 2. The surface scanning electron microscopy (SEM)–energy dispersive X-ray (EDX) micrographs of the PES/ZnO film photocatalysts by varying weight percentages of ZnO in the polymer solutions, (**a**,**b**) 0%, (**c**,**d**) 9%, (**e**,**f**) 17%, and (**g**,**h**) 19%.

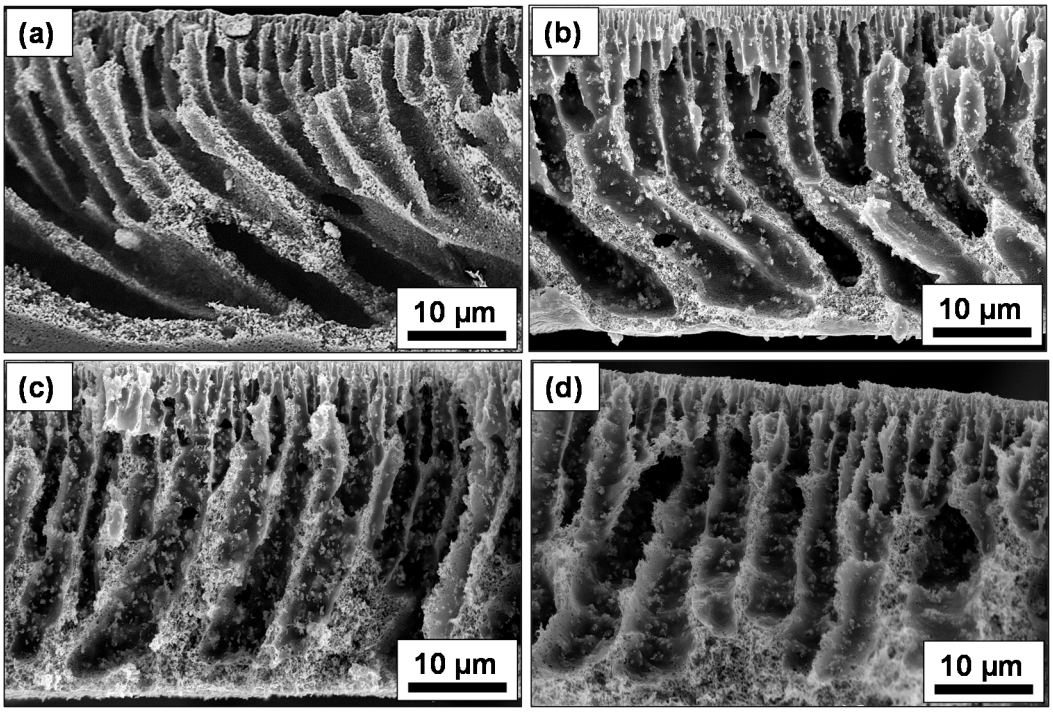

Figure 3. The cross-sectional SEM micrographs of PES/ZnO film photocatalysts with different ZnO loading, (**a**) PZ-0; (**b**) PZ-9; (**c**) PZ-17; and (**d**) PZ-19.

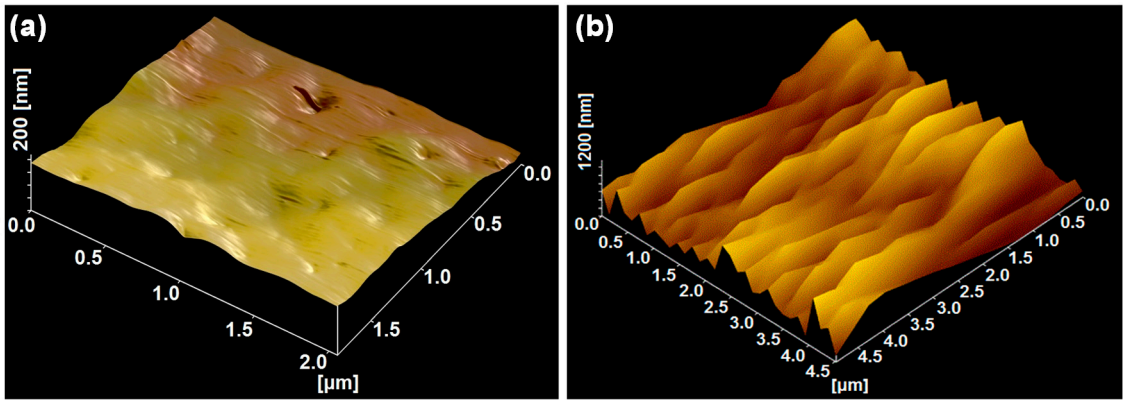

Figure 4. Three-dimensional atomic force microscopy (AFM) photographs of the surface layer of (**a**) PZ-0 and (**b**) PZ-17.

2.3. X-ray Photoelectron and Optical Property Analysis

XPS analysis was employed to examine the chemical state and surface conformation of the hybrid film photocatalyst. Figure 5 displays the wide scan spectrum of PZ-17 in the C 1s, O 1s, S 2p, and Zn 2p regions. The peaks observed in the XPS spectrums of C 1s at binding energies of 284.6 and 286.2 eV were assigned to the adventitious carbon (C–C) species and the C–S bonding in the PES matrix, respectively [29]. The XPS spectrum of O 1s of PES/ZnO (Figure 5c) was deconvoluted into four individual component peaks. The energy at 530.2 eV was consigned to the oxygen ions in the Zn–O–Zn bonding of the hexagonal wurtzite structure of the ZnO lattice. Distinctly higher binding energies at 531.5 and 532.7 eV were associated with the O=S=O and C–O groups of the PES film, respectively. The latter peak at 533.3 eV was consigned to chemisorbed or surface hydroxyl bonding of Zn–OH [30,31].

The XPS spectrums of S 2p displayed two binding energies at 168.7 and 167.5 eV (Figure 5d). The former peak was correlated with the sulfone (O=S=O) species [30], while the latter can be ascribed to the interaction of hydrogen bonding between the sulfone group and the superficial hydroxyl groups (–OH) of ZnO. These hydrogen bonding interactions are believed to be the cause of the well dispersed ZnO in the PES matrix as shown in the SEM micrographs. The peaks for Zn $2p_{3/2}$ and Zn $2p_{1/2}$ (Figure 5e) were observed at binding energies of 1021.0 eV and 1043.8 eV, respectively. The difference between Zn $2p_{3/2}$ and Zn $2p_{1/2}$ splitting was 22.8 eV (~23 eV) which corresponded with the standard value of ZnO indicating the presence of Zn^{2+} species in the PES/ZnO matrix [32].

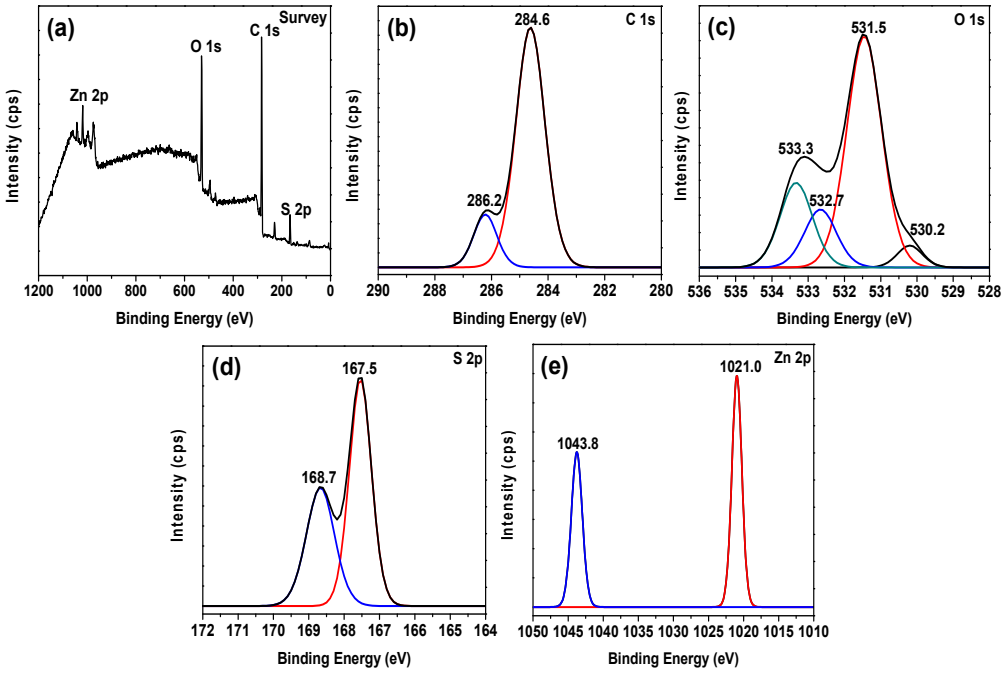

Figure 5. (**a**) X-ray photoelectron spectrums (XPS) survey spectrum and high resolution spectrums of (**b**) C 1s, (**c**) O 1s, (**d**) S 2p, and (**e**) Zn 2p of PES/ZnO (PZ-17) hybrid film photocatalyst.

The study on optical response of resultant PES/ZnO (PZ-17) sample and its correlation with the UV light was carried out using UV–Vis Diffuse Reflectance Spectroscopy. The absorption pattern and band gap energy measurement of the prepared PZ-17 hybrid film photocatalyst is illustrated in Figure 6. The photocatalyst's band gap was evaluated by constructing a graph according to $\alpha hv = A(hv - E_g)^2$, where α is an absorption coefficient, A is a constant, hv is the energy of a photon, E_g is the optical band gap [33]. The hv was derived from $hv = hc/\lambda$, where h is the Planck constant (4.136×10^{-15} eV), c is the velocity of the light in vacuum (2.977×1017 nm/s), and λ is the wavelength (nm). By extrapolating the linear section of the absorption edge, as presented in Figure 6, the energy gap of the photocatalyst was estimated. The prepared sample exhibited high optical responses against UV irradiation with a band gap of 3.15 eV and thus proved its effective application as a UV light active photocatalyst. The energy provided by the UV light lamp was 3.40 eV (λ = 365 nm), which is sufficient for the photoexcitation of the electrons to have occurred during the photodegradation of methyl orange.

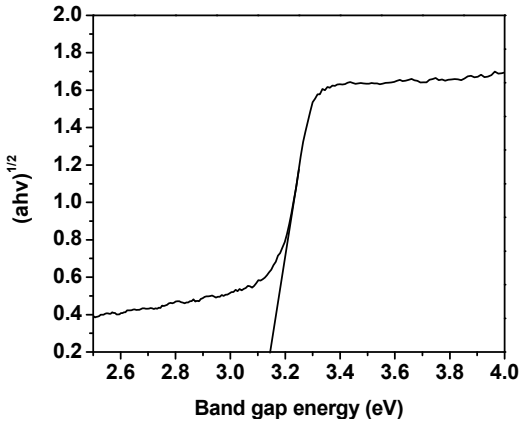

Figure 6. Optical property of the PZ-17 hybrid film photocatalyst.

2.4. Photocatalytic Degradation Activity by the PES/ZnO Hybrid Film Photocatalysts

Figure 7 shows the degradation of MO via photolysis and photocatalytic degradation by the PES/ZnO film photocatalysts. Preliminary studies revealed the adsorption of MO on neat PES was 0.80% but increased slightly to 2.76% when ZnO was incorporated into the PES film (PZ-17). The slight increase in MO could be attributed to the adsorption of MO on ZnO nanoparticles and the presence of porous structures in the PES/ZnO film photocatalysts. No significant degradation in the MO and pristine PES film (PZ-0) was observed during photolysis demonstrating the stability of MO and the incapability of PES to degrade MO during UV light irradiation. The performance of the photocatalysts and the degradation rate of MO were enhanced by the incorporation of ZnO nanoparticles up to 17 wt% (PZ-17), resulting in a maximum degradation percentage of 98% (Figure 7a,c). Higher content of ZnO nanoparticles immobilized onto the PES led to an increase in the availability of surface active sites for the photodegradation to take place. Additionally, the film photocatalyst surface containing more active sites offers better absorption of photon energy from UV light irradiation and thus, improved the photodegradation of MO. Figure 7c shows that even at a higher ZnO content (19 wt%), the degradation percentage and rate of reaction reduced significantly due to the agglomeration of ZnO nanoparticles subsequently reducing the available surface area and inefficient light absorption activity [34].

The effectiveness of the PES/ZnO film photocatalysts in the degradation of MO might also be related to their porous structures and surface roughness. The porous structure of the films was beneficial for light reflection [35], and provided a channel for the MO molecules to adsorb on the surface of the ZnO incorporated in the polymer matrix. The high surface roughness of the films improved their hydrophilic properties thus enhancing the interaction of the films with water, oxygen, and the contaminants [36]. Both properties provided favorable conditions for an efficient photodegradation process.

The efficiency of the PES/ZnO film photocatalyst was also found to be higher than that of previously reported PES/TiO_2 film photocatalyst. At the same metal oxide loading of 13 wt%, PES/TiO_2 film photocatalyst was able to degrade 80% of 10 ppm MO dye [19] compared to 95% by PES/ZnO within 9 h of irradiation time. The effectiveness of the PES/ZnO may be due to its higher surface roughness and better dispersion of ZnO particle inside the polymer matrix which prevent non-selective void formation in the polymer/nanoparticles interfaces. In other words, there is no potential for ZnO nanoparticles to fuse together inherently to form agglomeration and thus contribute to the individual dispersion and better pore formation as compared to TiO_2 particles [37]. Smaller particle size of ZnO as compared to TiO_2 also contributed to the formation of a higher degree of surface roughness. It is noteworthy to mention that high surface roughness of the films improved their hydrophilic properties thus enhancing the interaction of the film photocatalysts with water, oxygen and the contaminant molecules.

A heterogeneous photocatalytic reaction can be analyzed using the Langmuir–Hinshelwood (L–H) kinetic model as per Equation (1):

$$r = -\frac{dC}{dt} = k_{obs}C \quad (1)$$

By integrating Equation (1), a typical pseudo first-order equation was obtained as follows:

$$\ln \frac{C_o}{C} = k_{obs}C \quad (2)$$

where k_{obs} is the apparent pseudo first-order rate constant, C = MO concentration in the solution at a given irradiation time t, C_o = initial MO concentration. Figure 7b shows a straight line graph indicating that the photodegradation of MO by the PES/ZnO film photocatalysts followed a pseudo first-order kinetics. The progress of MO degradation was also monitored via the total organic carbon (TOC) concentration. Figure 7d shows that 80% of the organic carbon was degraded after 9 h of irradiation time. This value was 18% lower than that obtained from UV–Vis analysis indicating the presence of stable intermediates such as phenol, aniline, benzene sulfonic acid or benzene [10,38,39] that require a longer time to be degraded by the photocatalyst.

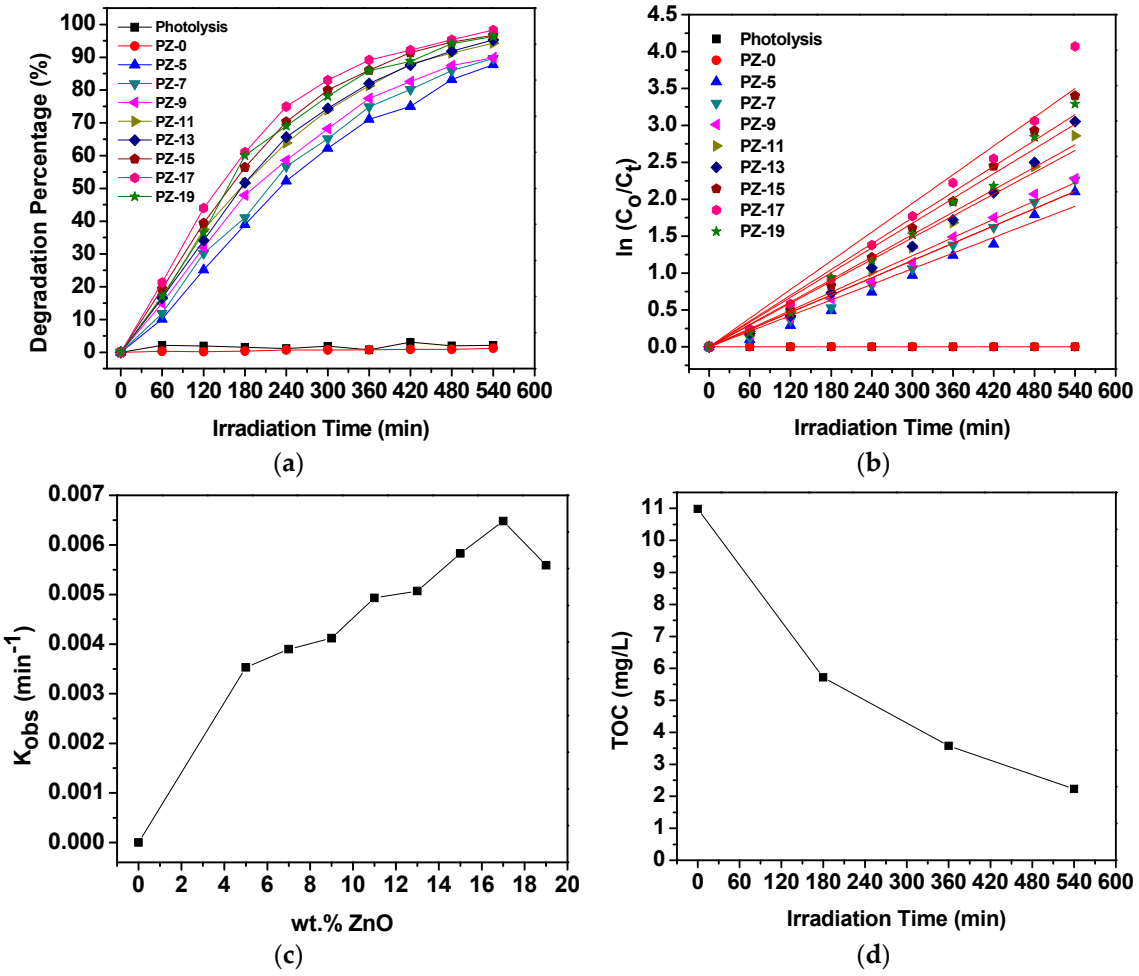

Figure 7. (**a**) Degradation percentages and (**b**) kinetics of the degradation of methyl orange (MO) by the PES/ZnO film photocatalysts with different ZnO loading (0–19 wt%), (**c**) first-order rate constant, and (**d**) total organic carbon (TOC) evaluation for the concentrations of MO. [MO] = 10 mg/L; pH = 5.8; quantity of films = 2.

2.5. Effect of Variables in the Operating Parameters on the Degradation Percentage of MO

As illustrated in Figure 8a,b, the degradation rate improves as more than two films are placed into the photoreactor. A complete degradation of MO was obtained in a much shorter irradiation time (7 h) when four pieces of film were used compared to others (9 h). Contrary to the slurry method which exhibited declining efficiency at higher photocatalyst loading due to particle aggregation, poor light penetration, and light scattering [40,41], the photoactivity of the film photocatalyst increased with an increasing quantity of films due to the higher availability of ZnO particles immobilized in the polymer matrix. The degradation rate and amount of MO degraded by using several numbers of PZ-17 film photocatalysts are listed in Table 1.

The efficiency of the PZ-17 film in the photodegradation of MO at certain pHs varying from 2 to 10 is further depicted in Figure 8c,d. The degradation rate and the degradation percentage increased significantly when the pH of the solution altered from 2 to 4, then remained almost unchanged with increasing pH values up to pH 8 after which it reduced slightly at pH 10. In order to explain this, the interaction between the surface of the photocatalyst and the dye at different pHs was correlated. Accordingly, the point zero charge (pH_{pzc}) of ZnO was 9.0 and thus, its surface became positively charged and negatively charged at pHs below and above 9.0, respectively as shown in Equations (3) and (4) [42]. It has also been reported that the pKa of MO is 3.46 [43].

$$ZnOH + H^+ \rightarrow ZnOH_2{}^+ \left(pH < pH_{pzc}\right) \quad (3)$$

$$ZnOH + OH^- \rightarrow ZnO^- + H_2O \left(pH > pH_{pzc}\right) \quad (4)$$

At pH 2, the MO molecules became protonated, therefore a repulsive force existed between the positively charged MO molecules and positively charged ZnO surface. Consequently, the rate and the degradation percentage of MO at pH 2 was observed to be very low as tabulated in Table 2. When increasing the pH of the solution (pH 4–8), the MO molecules became negatively charged and were attracted to the positively charged ZnO surface, resulting in an increase in the rate and degradation percentage of MO. At pH 10, the existence of a repulsive force between the negatively charged ZnO surface and negatively charged MO contributed to a slight decrease in the degradation rate and degradation percentage of MO. The film did not experience significant weight loss demonstrating the stability of the PES/ZnO film photocatalyst in acidic or basic conditions, hence proving the ability of the film photocatalyst to work under various pHs of real wastewaters.

The photocatalytic degradation performance of PZ-17 was further evaluated on the effect of initial MO concentrations. As shown in Table 3, the degradation rate and the amount of MO degraded were found to increase in parallel with increasing MO concentration. This proved that the photoactivity of the film was not affected by the concentration of MO up to 20 mg/L, indicating the effectiveness of the PZ-17 film in degrading higher concentrations of MO.

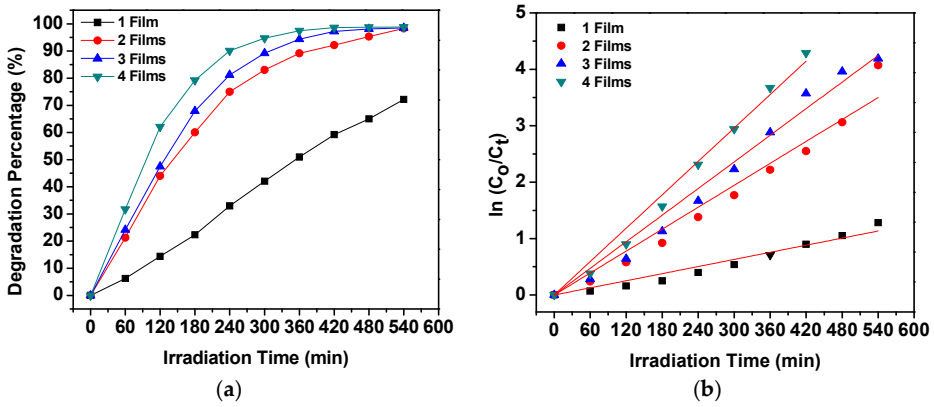

Figure 8. *Cont.*

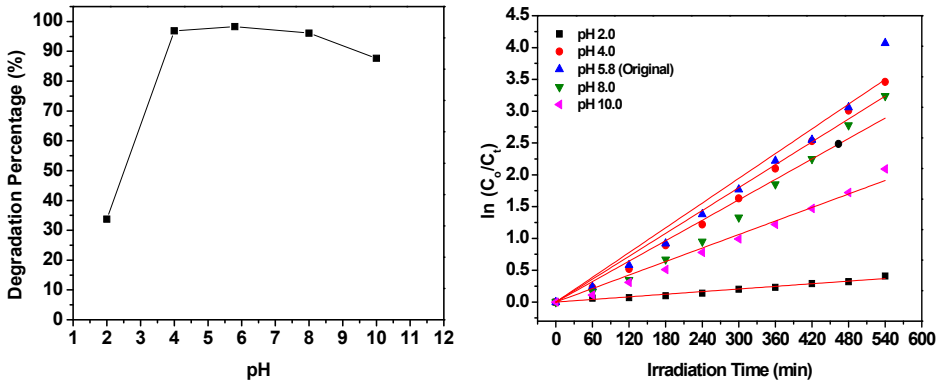

Figure 8. (**a**,**b**) The effect of the quantity of films and (**c**,**d**) the effect of initial pHs on the degradation percentage and kinetics of the degradation of MO by the PZ-17 film photocatalyst.

Table 1. Kinetic data and the amount of methyl orange (MO) degraded at different quantity of film by the PZ-17 film photocatalyst.

Quantity of Film	Degradation Percentage (%)	k_{obs} (min^{-1})	Rate (mg/L min)	Amount of MO Degraded (mg/g)	Correlation Factor, R^2
1	72.16	0.00210	0.02090	17.83	0.98251
2	98.28	0.00648	0.06798	25.60	0.98591
3	98.49	0.00786	0.07805	25.67	0.99328
4	98.82	0.00987	0.09395	25.74	0.99520

Table 2. Kinetic data and the amount of MO degraded at different initial pH by the PZ-17 film photocatalyst.

Initial pH of MO Solution	Degradation Percentage (%)	k_{obs} (min^{-1})	Rate (mg/L min)	Amount of MO Degraded (mg/g)	Correlation Factor, R^2
2.0	33.75	0.00069	0.00734	15.24	0.99167
4.0	96.85	0.00599	0.06079	24.40	0.99283
5.8 (original)	98.28	0.00648	0.06798	25.60	0.98591
8.0	96.09	0.00535	0.05612	25.02	0.97931
10.0	87.69	0.00354	0.03738	22.99	0.99267

Table 3. Kinetic data and the amount of MO degraded at different initial concentration by the PZ-17 film photocatalyst.

Initial Concentration of MO Solution (mg/L)	Degradation Percentage (%)	k_{obs} (min^{-1})	Rate (mg/L min)	Amount of MO Degraded (mg/g)	Correlation Factor, R^2
5	99.41	0.00922	0.04665	12.49	0.99766
10	98.28	0.00648	0.06798	25.60	0.98591
15	93.96	0.00474	0.07063	34.76	0.98936
20	90.60	0.00403	0.08020	44.76	0.99208

2.6. Recyclability

The recyclability of the PES/ZnO (PZ-17) hybrid film photocatalyst for MO degradation was investigated, by adding fresh MO aqueous solution to the new cycle after earlier reaction cessation, without undergoing any physical or chemical pretreatment of the film for every cycle. The amount of MO degraded and degradation percentage results as a function of reaction time for five consecutive cycles are displayed comparatively in Table 4 and Figure 9, respectively. Noticeably, the investigated

film exhibited high degradation activity, without any significant loss in its photacatalytic performance even after five consecutive cycles. In comparison with the recyclability and efficiency of the best PES/TiO_2 (PT-13) hybrid film photocatalyst previously reported [19], the degradation percentage was achieved at the most of 80% which also displayed a comparable result over five cycles. The different photocatalytic performance displayed by both types of film photocatalysts might be due to the particle size of the nanoparticles. The particle size for ZnO was in the range of 1–100 nm while TiO_2 was in the range of 1–150 nm. The smaller particle size of ZnO is more advantageous for the effective dispersion within the polymer matrix, providing a higher surface area and thus maximizing the utilization of photon energy from UV light [44,45]. Therefore, it can be concluded that the results obtained in this study display the stability and credibility of the PES–nanoparticles hybrid film against UV irradiation and are potentially useful for the photocatalytic water remediation process.

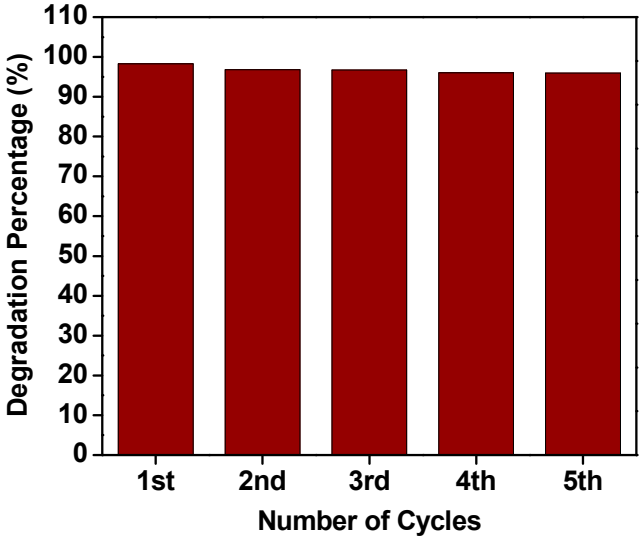

Figure 9. Recyclability test of the PZ-17 film in the photocatalytic degradation of MO. [MO] = 10 mg/L; pH = 5.8; quantity of films = 2.

Table 4. The amount of MO degraded in 5 consecutive cycles using the PZ-17 film photocatalyst.

Number of Cycle	Irradiation Time (h)	Degradation Percentage (%)	Amount of MO Degraded (mg/g)
1	9	98.28	25.60
2	18	96.79	25.49
3	27	96.70	25.49
4	36	95.98	25.45
5	45	95.95	25.32

3. Experimental

3.1. Materials

Methyl orange (MO), *N*-methyl-2-pyrrolidone (NMP) and polyethersulfone (Ultrason E6020P with M_w = 75,000 g/mol) were procured from Bendosen Laboratory Chemical (Batu Caves, Malaysia), Merck (Petaling Jaya, Malaysia) and Solvay Specialty Polymers (Brussels, Belgium), respectively. A readily available zinc oxide (particle size: 1–100 nm, purity >99%) was obtained from a commercial brand (Merck). All chemicals and reagents received were analytical grade and no purification step was executed. Distilled water (18.2 MΩ cm resistivity) was utilized for all the experiments.

3.2. Preparation of the PES/ZnO Hybrid Film Photocatalysts

Polyethersulfone-ZnO film photocatalysts were prepared in accordance with our previously reported methodology [19]. Briefly, the PES casting solution was prepared by dissolving a fixed amount of polymer resin in the organic solvent (NMP) followed by mixing certain amounts of ZnO nanoparticles into the crystal clear polymeric solution. The compositions of the prepared films are tabulated in Table 5. A uniform dispersion of ZnO in the PES solutions was attained after continuously stirring for 24 h at ambient temperature. The final mixture was cast on a flat glass (10 cm × 8 cm) using a casting knife with 100 μm gap setting at an appropriate casting shear. The glass plate with a film on top of it was then immersed in a non-solvent media (distilled water) and the prepared film was stored for 1 day to achieve a thorough phase separation with the removal of the remaining solvents. Lastly, the resultant films were air-dried at ambient temperature for 24 h prior to the initiation of photocatalytic degradation activity studies.

Table 5. The compositions of casting solution of polyethersulfone (PES)/ZnO film photocatalysts. NMP = *N*-methyl-2-pyrrolidone.

PES wt%	ZnO wt%	NMP wt%	Labelled as
15	0	85	PZ-0
15	5	80	PZ-5
15	7	78	PZ-7
15	9	76	PZ-9
15	11	74	PZ-11
15	13	72	PZ-13
15	15	70	PZ-15
15	17	68	PZ-17
15	19	66	PZ-19

3.3. Characterization of the PES/ZnO Hybrid Film Photocatalysts

The crystallinity of prepared PES/ZnO film photocatalysts was determined using an X-ray diffraction (PHILIPS PW 3040/60) analysis (Philips, Petaling Jaya, Malaysia) with a CuKα radiation of wavelength 0.15406 nm and beam intensity of 30 mA and 30 kV. The diffracted intensity was scanned in a range of 2θ = 20–80° with 2°/min of scanning speed. Surface morphological and cross-section comparison of the prepared films were analyzed by a scanning electron microscopy fitted with an energy dispersive X-ray analyzer (HITACHI TM3000) (Hitachi, Kuala Lumpur, Malaysia) and atomic force microscopy (Seiko Instruments SPI 3800N, Contact mode). The band gap energy of the prepared films was determined using a UV–Vis Diffuse Reflectance Spectrometer (UV-3101PC Shimadzu, Maximum resolution: 0.1 nm) (Shimadzu, Petaling Jaya, Malaysia). A Kratos Analytical Axis Ultra DLD photoelectron spectrometer with Al Kα radiation monochromatic source was employed to elucidate the X-ray photoelectron spectrums (XPS) (UKM, Bangi, Malaysia) of the prepared film. The pass energy (PE) used for XPS measurement was 160 eV (survey scan) and 20 eV (narrow scan). The porosity (ε) of the prepared films was calculated by employing a gravimetric technique as formulated in Equation (5) below:

$$\varepsilon(\%) = \frac{\frac{(W_w - W_d)}{\rho_H}}{\frac{(W_w - W_d)}{\rho_H} + \frac{W_d}{\rho_p}} \quad (5)$$

where W_d and W_w are the weight of dry and wet membranes (g), respectively. ρ_p is the density of polyethersulfone (0.25 g/cm^3) and ρ_H is the density of water (0.998 g/cm^3).

3.4. Photocatalytic Degradation Procedure

The photodegradation of MO was carried out in an immersion well photoreactor. The features of the photoreactor were described in a recent publication [19]. Two units of the PES/ZnO hybrid film photocatalysts (10 cm × 8 cm) were positioned near the quartz cylinder. MO solution (1000 mL) with known concentration was poured into the reactor. Air was fed into the reactor containing MO solution to warrant a consistent source of oxygen with a fixed flow rate of 4 L/min. The first 20 min of the reaction was spent in reaching adsorption–desorption equilibrium by continuous stirring of the solution under dark conditions, prior to irradiation by a 6-watt UV-A lamp (HITACHI F6T5/BL) (Hitachi, Kuala Lumpur, Malaysia) for 540 min. An aliquot sample of 10 mL was taken out at certain time intervals and the concentration of MO left was determined using a UV–Vis Spectrometer (PerkinElmer Lambda 35) (Perkin Elmer, Petaling Jaya, Malaysia) at λ_{max} = 464 nm. The total organic carbon study was performed by TOC analyzer (TOC-V-E, Shimadzu, Petaling Jaya, Malaysia). The photocatalytic degradation percentage and the amount of MO degraded were calculated based on Equations (6) and (7), respectively;

$$\text{Degradationpercentage}\ (\%) = \frac{(C_o - C_t)}{C_o} \times 100\% \quad (6)$$

$$\text{Amount of MO degraded}\ (\text{mg/g}) = \frac{(C_o - C_t)\left(\frac{\text{mg}}{\text{L}}\right) \times \text{volume}\ (\text{L})}{\text{weight of PES/ZnO film}\ (\text{g})} \quad (7)$$

where C_o is the concentration of methyl orange (MO) before irradiation and C_t is the concentration of MO at time '*t*'.

The variables such as the quantity of films, initial pH, and initial concentrations of the MO solution on the photodegradation of MO were investigated using the PZ-17 film photocatalyst. In this study, a total of four pieces of film were used to investigate the effect of using different quantity of films since the maximum capacity of films that can be put inside the reactor is only four. The initial pH of the MO solution was determined as ranging from 2 to 10 and the initial concentration used was selected in the range of 5 to 20 ppm. The recyclability of the PZ-17 film in the photodegradation of MO was studied using a concentration of 10 mg/L at pH 5.8 and irradiated under a UV-A lamp for a period of 9 h. The film photocatalyst was cleaned with distilled water for every cycle and then used to treat fresh MO aqueous solution.

4. Conclusions

PES/ZnO film photocatalysts were successfully synthesized by immobilizing ZnO into PES film by means of a phase inversion method. The best degradation percentage of 98% was obtained when two pieces of PES-17 wt% of ZnO (PZ-17) film photocatalysts (10 cm × 8 cm) were tested to degrade 10 mg/L of MO solution at the original pH of 5.8 with the amount of MO degraded achieved at 25.60 mg/g. Increasing the concentration of MO up to 20 ppm reduced the degradation percentage to 90%. Increasing the quantity of films from two to four exhibited a comparable degradation percentage of 98%. The PZ-17 film photocatalyst showed good stability when exposed to UV irradiation and could be used in aggressive basic and acidic media. The PZ-17 film photocatalyst maintained its high level degradation performance up to five cycles, without itself being treated with any regeneration process.

Acknowledgments: The authors gratefully acknowledge the financial support from the Ministry of Higher Education for the FRGS-GSP grant and a scholarship award under the MyBrain15 scheme (Zul Adlan), Universiti Putra Malaysia and Universiti Kebangsaan Malaysia (XPS) for the technical and management support to conduct the research work.

Author Contributions: Zul Adlan Mohd Hir and Abdul Halim Abdullah conceived, designed, and performed the experiments; Zul Adlan Mohd Hir, Abdul Halim Abdullah, Zulkarnain Zainal, and Hong Ngee Lim analyzed the data; and Zul Adlan Mohd Hir wrote the paper.

Conflicts of Interest: The authors declare no conflicts of interest.

References

1. Miranda-García, N.; Suárez, S.; Sánchez, B.; Coronado, J.M.; Malato, S.; Maldonado, I.M. Photocatalytic degradation of emerging contaminants in municipal wastewater treatment plant effluents using immobilized TiO_2 in a solar pilot plant. *Appl. Catal. B Environ.* **2011**, *103*, 294–301. [CrossRef]
2. Vaiano, V.; Matarangolo, M.; Sacco, O.; Sannino, D. Photocatalytic treatment of aqueous solutions at high dye concentration using praseodymium-doped ZnO catalysts. *Appl. Catal. B Environ.* **2017**, *209*, 621–630. [CrossRef]
3. May-Lozano, M.; Mendoza-Escamilla, V.; Rojas-García, E.; López-Medina, R.; Rivadeneyra-Romero, G.; Martinez-Delgadillo, S.A. Sonophotocatalytic degradation of Orange II dye using low cost photocatalyst. *J. Clean. Prod.* **2017**, *148*, 836–844. [CrossRef]
4. Bailón-García, E.; Elmouwahidi, A.; Álvarez, M.A.; Carrasco-Marín, F.; Pérez-Cadenas, A.F.; Maldonado-Hódar, F.J. New carbon xerogel-TiO_2 composites with high performance as visible-light photocatalysts for dye mineralization. *Appl. Catal. B Environ.* **2017**, *201*, 29–40. [CrossRef]
5. Intarasuwan, K.; Amornpitoksuk, P.; Suwanboon, S.; Graidist, P. Photocatalytic dye degradation by ZnO nanoparticles prepared from $X_2C_2O_4$ (X = H, Na and NH_4) and the cytotoxicity of the treated dye solutions. *Sep. Purif. Technol.* **2017**, *177*, 304–312. [CrossRef]
6. Chowdhury, S.; Balasubramanian, R. Recent advances in the use of graphene-family nanoadsorbents for removal of toxic pollutants from wastewater. *Adv. Colloid Interface Sci.* **2014**, *204*, 35–56. [CrossRef] [PubMed]
7. Riera-Torres, M.; Gutiérrez-Bouzán, C.; Crespi, M. Combination of coagulation-flocculation and nanofiltration techniques for dye removal and water reuse in textile effluents. *Desalination* **2010**, *252*, 53–59. [CrossRef]
8. Ghaedi, M.; Sadeghian, B.; Pebdani, A.A.; Sahraei, R.; Daneshfar, A.; Kinetics, C.D. thermodynamics and equilibrium evaluation of direct yellow 12 removal by adsorption onto silver nanoparticles loaded activated carbon. *Chem. Eng. J.* **2012**, *187*, 133–141. [CrossRef]
9. Bagheri, S.; Hir, Z.A.M.; Yousefi, A.T.; Hamid, S.B.A. Progress on mesoporous titanium dioxide: Synthesis, modification and applications. *Microporous Mesoporous Mater.* **2015**, *218*, 206–222. [CrossRef]
10. Kaur, J.; Singhal, S. Facile synthesis of ZnO and transition metal doped ZnO nanoparticles for the photocatalytic degradation of Methyl Orange. *Ceram. Int.* **2014**, *40*, 7417–7424. [CrossRef]
11. Siuleiman, S.; Kaneva, N.; Bojinova, A.; Papazova, K.; Apostolov, A.; Dimitrov, D. Photodegradation of Orange II by ZnO and TiO_2 powders and nanowire ZnO and ZnO/TiO_2 thin films. *Colloids Surf. A Physicochem. Eng. Asp.* **2014**, *460*, 408–413. [CrossRef]
12. Chaker, H.; Chérif-Aouali, L.; Khaoulani, S.; Bengueddach, A.; Fourmentin, S. Photocatalytic degradation of methyl orange and real wastewater by silver doped mesoporous TiO_2 catalysts. *J. Photochem. Photobiol. A Chem.* **2016**, *318*, 142–149. [CrossRef]
13. Dong, H.; Zeng, G.; Tang, L.; Fan, C.; Zhang, C.; He, X.; He, Y. An overview on limitations of TiO_2-based particles for photocatalytic degradation of organic pollutants and the corresponding countermeasures. *Water Res.* **2015**, *79*, 128–146. [CrossRef] [PubMed]
14. Saadoun, M.; Chorfi, H.; Bousselmi, L.; Bessaïs, B. Polymer supported porous TiO_2: Application to photo-catalysis. *Phys. Status Solidi Curr. Top. Solid State Phys.* **2007**, *4*, 2029–2033. [CrossRef]
15. Singh, S.; Mahalingam, H.; Singh, P.K. Polymer-supported titanium dioxide photocatalysts for environmental remediation: A review. *Appl. Catal. A Gen.* **2013**, *462–463*, 178–195. [CrossRef]
16. Vaiano, V.; Sarno, G.; Sacco, O.; Sannino, D. Degradation of terephthalic acid in a photocatalytic system able to work also at high pressure. *Chem. Eng. J.* **2017**, *312*, 10–19. [CrossRef]
17. Mozia, S.; Darowna, D.; Wróbel, R.; Morawski, A.W. A study on the stability of polyethersulfone ultrafiltration membranes in a photocatalytic membrane reactor. *J. Membr. Sci.* **2015**, *495*, 176–186. [CrossRef]
18. Fischer, K.; Kühnert, M.; Gläser, R.; Schulze, A. Photocatalytic degradation and toxicity evaluation of diclofenac by nanotubular titanium dioxide–PES membrane in a static and continuous setup. *RSC Adv.* **2015**, *5*, 16340–16348. [CrossRef]
19. Hir, Z.A.M.; Moradihamedani, P.; Abdullah, A.H.; Mohamed, M.A. Immobilization of TiO_2 into polyethersulfone matrix as hybrid film photocatalyst for effective degradation of methyl orange dye. *Mater. Sci. Semicond. Process.* **2017**, *57*, 157–165. [CrossRef]

20. Pardeshi, S.K.; Patil, A.B. Solar photocatalytic degradation of resorcinol a model endocrine disrupter in water using zinc oxide. *J. Hazard. Mater.* **2009**, *163*, 403–409. [CrossRef] [PubMed]
21. Yan, H.; Hou, J.; Fu, Z.; Yang, B.; Yang, P.; Liu, K.; Wen, M.; Chen, Y.; Fu, S.; Li, F. Growth and photocatalytic properties of one-dimensional ZnO nanostructures prepared by thermal evaporation. *Mater. Res. Bull.* **2009**, *44*, 1954–1958. [CrossRef]
22. Bindu, P.; Thomas, S. Estimation of lattice strain in ZnO nanoparticles: X-ray peak profile analysis. *J. Theor. Appl. Phys.* **2014**, *8*, 123–134. [CrossRef]
23. Yin, J.; Deng, B. Polymer-matrix nanocomposite membranes for water treatment. *J. Membr. Sci.* **2014**, 1–20. [CrossRef]
24. Rajabi, H.; Ghaemi, N.; Madaeni, S.S.; Daraei, P.; Astinchap, B.; Zinadini, S.; Hossein, S. Nano-ZnO embedded mixed matrix polyethersulfone (PES) membrane: Influence of nanofiller shape on characterization and fouling resistance. *Appl. Surf. Sci.* **2015**, *349*, 66–77. [CrossRef]
25. Li, X.; Fang, X.; Pang, R.; Li, J.; Sun, X.; Shen, J.; Han, W.; Wang, L. Self-assembly of TiO_2 nanoparticles around the pores of PES ultrafiltration membrane for mitigating organic fouling. *J. Membr. Sci.* **2014**, *467*, 226–235. [CrossRef]
26. De Sitter, K.; Dotremont, C.; Genne, I.; Stoops, L. The use of nanoparticles as alternative pore former for the production of more sustainable polyethersulfone ultrafiltration membranes. *J. Membr. Sci.* **2014**, *471*, 168–178. [CrossRef]
27. Shen, L.; Bian, X.; Lu, X.; Shi, L.; Liu, Z.; Chen, L.; Hou, Z.; Fan, K. Preparation and characterization of ZnO/polyethersulfone (PES) hybrid membranes. *Desalination* **2012**, *293*, 21–29. [CrossRef]
28. Ahmad, A.L.; Abdulkarim, A.A.; Shafie, Z.M.H.M.; Ooi, B.S. Fouling evaluation of PES/ZnO mixed matrix hollow fiber membrane. *Desalination* **2017**, *403*, 53–63. [CrossRef]
29. Wavhal, D.S.; Fisher, E.R. Membrane surface modification by plasma-induced polymerization of acrylamide for improved surface properties and reduced protein fouling. *Langmuir* **2003**, *19*, 79–85. [CrossRef]
30. Liu, S.X.; Kim, J.-T. Characterization of Surface Modification of Polyethersulfone Membrane. *J. Adhes. Sci. Technol.* **2011**, *25*, 193–212. [CrossRef]
31. Zhang, X.; Qin, J.; Xue, Y.; Yu, P.; Zhang, B.; Wang, L.; Liu, R. Effect of aspect ratio and surface defects on the photocatalytic activity of ZnO nanorods. *Sci. Rep.* **2014**, *4*, 1–8. [CrossRef] [PubMed]
32. Al-gaashani, R.; Radiman, S.; Daud, A.R.; Tabet, N.; Al-Douri, Y. XPS and optical studies of different morphologies of ZnO nanostructures prepared by microwave methods. *Ceram. Int.* **2013**, *39*, 2283–2292. [CrossRef]
33. Mohamed, M.A.; Salleh, W.N.W.; Jaafar, J.; Rosmi, M.S.; Hir, Z.A.M.; Mutalib, M.A.; Ismail, A.F.; Tanemura, M. Carbon as amorphous shell and interstitial dopant in mesoporous rutile TiO_2: Bio-template assisted sol-gel synthesis and photocatalytic activity. *Appl. Surf. Sci.* **2017**, *393*, 46–59. [CrossRef]
34. Lei, P.; Wang, F.; Gao, X.; Ding, Y.; Zhang, S.; Zhao, J.; Liu, S.; Yang, M. Immobilization of TiO_2 nanoparticles in polymeric substrates by chemical bonding for multi-cycle photodegradation of organic pollutants. *J. Hazard. Mater.* **2012**, *227–228*, 185–194. [CrossRef] [PubMed]
35. Zyoud, A.; Zu'bi, A.; Helal, M.H.S.; Park, D.; Campet, G.; Hilal, H.S. Optimizing photo-mineralization of aqueous methyl orange by nano-ZnO catalyst under simulated natural conditions. *J. Environ. Health Sci. Eng.* **2015**, *13*, 46. [CrossRef] [PubMed]
36. Mohamed, M.A.; Salleh, W.N.W.; Jaafar, J.; Ismail, A.F.; Mutalib, M.A.; Sani, N.A.A.; Asri, S.E.A.M.; Ong, C.S. Physicochemical characteristic of regenerated cellulose/N-doped TiO_2 nanocomposite membrane fabricated from recycled newspaper with photocatalytic activity under UV and visible light irradiation. *Chem. Eng. J.* **2016**, *284*, 202–215. [CrossRef]
37. Moradihamedani, P.; Ibrahim, N.A.; Zin, W.; Yunus, W.; Yusof, N.A. Study of morphology and gas separation properties of polysulfone/titanium dioxide mixed matrix membranes. *Polym. Eng. Sci.* **2015**, 367–374. [CrossRef]
38. Xie, S.; Huang, P.; Kruzic, J.J.; Zeng, X.; Qian, H. A highly efficient degradation mechanism of methyl orange using Fe-based metallic glass powders. *Sci. Rep.* **2016**, *6*, 1–10. [CrossRef] [PubMed]
39. Jaafar, N.F.; Jalil, A.A.; Triwahyono, S.; Muhid, M.N.M.; Sapawe, N.; Satar, M.A.H.; Asaari, H. Photodecolorization of methyl orange over α-Fe_2O_3-supported HY catalysts: The effects of catalyst preparation and dealumination. *Chem. Eng. J.* **2012**, *191*, 112–122. [CrossRef]

40. Zhang, L.; Li, N.; Jiu, H.; Qi, G.; Huang, Y. ZnO-reduced graphene oxide nanocomposites as efficient photocatalysts for photocatalytic reduction of CO_2. *Ceram. Int.* **2015**, *41*, 6256–6262. [CrossRef]
41. Zhang, L.; Tse, M.S.; Tan, O.K. Facile in situ synthesis of visible light-active Pt/C-TiO_2 nanoparticles for environmental remediation. *J. Environ. Chem. Eng.* **2014**, *2*, 1214–1220. [CrossRef]
42. Saleh, R.; Djaja, N.F. Transition-metal-doped ZnO nanoparticles: Synthesis, characterization and photocatalytic activity under UV light. *Spectrochim. Acta Part A Mol. Biomol. Spectrosc.* **2014**, *130*, 581–590. [CrossRef] [PubMed]
43. Subbaiah, M.V.; Kim, D.S. Adsorption of methyl orange from aqueous solution by aminated pumpkin seed powder: Kinetics, isotherms, and thermodynamic studies. *Ecotoxicol. Environ. Saf.* **2016**, *128*, 109–117. [CrossRef] [PubMed]
44. Bagheri, S.; Hir, Z.A.M.; Yousefi, A.T.; Hamid, S.B.A. Photocatalytic performance of activated carbon-supported mesoporous titanium dioxide. *Desalin. Water Treat.* **2015**, 1–7. [CrossRef]
45. Mohamed, M.A.; Mutalib, M.A.; Hir, Z.A.M.; Zain, M.F.M.; Mohamad, A.B.; Minggu, L.J.; Awang, N.A.; Salleh, W.N.W. An overview on cellulose-based material in tailoring bio-hybrid nanostructured photocatalysts for water treatment and renewable energy applicationsm. *Int. J. Biol. Macromol.* **2017**, *103*, 1232–1256. [CrossRef] [PubMed]

© 2017 by the authors. Licensee MDPI, Basel, Switzerland. This article is an open access article distributed under the terms and conditions of the Creative Commons Attribution (CC BY) license (http://creativecommons.org/licenses/by/4.0/).